Applied Organometallic Chemistry

WILEY

Applied Organometallic Chemistry

RESEARCH ARTICLE

Co-Encapsulated Niosomes With Metformin and Silver Nanoparticles as Potential Anticancer Tool for the Combined Therapy on Lung Cancer Cells

Hamid Rashidzadeh[1] | Mahmoud Gharbavi[2,3] | Roghayeh Ghorbani[4,5] | Mahdis Nazari[6] | Hadi Noei[7] | Behrooz Johari[1,6]

[1]Zanjan Pharmaceutical Biotechnology Research Center, Zanjan University of Medical Sciences, Zanjan, Iran | [2]Nanotechnology Research Center, Medical Basic Sciences Research Institute, Ahvaz Jundishapur University of Medical Sciences, Ahvaz, Iran | [3]Pain Research Center, Ahvaz Jundishapur University of Medical Sciences, Ahvaz, Iran | [4]Cellular and Molecular Research Center, Cellular and Molecular Medicine Institute, Urmia University of Medical Sciences, Urmia, Iran | [5]Department of Applied Cell Sciences, Faculty of Medicine, Urmia University of Medical Sciences, Urmia, Iran | [6]Student Research Committee, School of Medicine, Zanjan University of Medical Sciences, Zanjan, Iran | [7]Department of Medical Biology and Genetics, Faculty of Medicine, Istinye University, Istanbul, Turkey

Correspondence: Mahmoud Gharbavi (gharbavi1981@gmail.com; gharbavi-m@ajums.ac.ir) | Behrooz Johari (behroozjohari@yahoo.com; dr.johari@zums.ac.ir)

Received: 4 December 2024 | **Revised:** 11 June 2025 | **Accepted:** 18 June 2025

Funding: Zanjan University of Medical Sciences supported the present study (Grant Number A-12-1244-29 and Ethical Code: IR.ZUMS.BLC.1402.050).

Keywords: combinational therapy | lung cancer | metformin | niosomes | silver nanoparticle

ABSTRACT

The present study aimed to develop niosomes (NISM) containing metformin (Met) drugs and silver nanoparticles (AgNPs) as radiosensitizer agents. Also, the combinational effect of Met drug and AgNPs in conjunction with x-irradiation exposure in both blank and Ag-Met encapsulated niosome (NISM and NISM@Ag-Met) forms on the suppression of cell growth and induction of apoptosis in lung cancer (A549) cell line were exploited. Niosomes were prepared by thin-film hydration method and loaded with AgNPs and Met drug. The prepared NISM@Ag-Met radiosensitizer was then characterized using various techniques including DLS, FTIR, UV–Vis, FE-SEM, and ICP-MS. The feasibility of NISM@Ag-Met nanosystems for cancer treatment was exploited using cell viability and apoptosis assay both with and without x-ray irradiation (4 Gy). Both in the presence and absence of x-ray irradiation, the encapsulation of AgNPs and Met medication in a niosomal formulation demonstrated reduced cell growth and promoted apoptosis; notably, the effects were more pronounced when combined with radiation therapy. It can be concluded that NISM@Ag-Met could serve as a radiosensitizer and a potential carrier for drug delivery in combined therapy against lung cancer cells. However, more research concentrating on in vivo tests is needed to confirm the effectiveness of developed NISM@Ag-Met nanosystems in cancer treatment.

Abbreviations: Ag, silver; AgNPs, silver nanoparticles; Au, gold; BSA, bovine serum albumin; DLS, dynamic light scattering; EE, encapsulation efficiency; FESEM, field emission scanning electron microscopy; FT-IR, Fourier transform infrared; GSH, glutathione; ICP-MS, inductively coupled plasma mass spectrometry; Met, metformin; NISM, niosomes; NSCLC, non–small cell lung cancer; PDI, polydispersity Index; PI, propidium iodide; Pt, platinum; ROS, reactive oxygen species; RT, radiation therapy; SCLC, small cell lung cancer; SDS, sodium dodecyl sulfate; UV–Vis, ultraviolet–visible.

Behrooz Johari and Hamid Rashidzadeh contributed equally to this work and hence are co-first authors.

1 | Introduction

Lung cancer is the leading cause of cancer-related deaths worldwide, accounting for approximately 1.8 million deaths annually [1]. The two most common types of lung cancer are small cell lung cancer (SCLC) and non–small cell lung cancer (NSCLC). Although SCLC is less common, it tends to spread and grow more rapidly, whereas NSCLC is more prevalent and often grows at a slower rate [2, 3]. NSCLC constitutes about 85% of all lung cancer cases and is often diagnosed at advanced stages, resulting in poor prognosis and limited survival rates [4].

Despite advancements in therapeutic modalities including radiation therapy (RT), chemotherapy, immunotherapy, and surgery, the 5-year survival rate for lung cancer patients remains extremely low. RT, as the cornerstone modality, is broadly used in both early and advanced lung cancer. Although RT is a potent tumor suppressor, the presence of radioresistant tumors diminishes its efficacy, resulting in suboptimal tumor control and a higher risk of recurrence [5, 6]. This clinical problem highlights the urgent need for strategies that can increase tumor cell susceptibility to radiation-induced damage.

Radiosensitizers have been developed as a solution to enhance the therapeutic impact of RT by sensitizing tumor cells to radiation [7]. These agents function by increasing DNA damage or generating reactive oxygen species (ROS) during irradiation, thereby amplifying the cytotoxic effects of RT [8]. Although several chemical radiosensitizers have been developed, conventional ones suffer from significant drawbacks, including systemic toxicity, poor tumor selectivity, and limited clinical success.

In recent years, metal-based nanoparticles (NPs) such as silver (Ag), gold (Au), and platinum (Pt) have emerged as promising radiosensitizers due to their high atomic number, which enables efficient absorption of x-ray energy and emission of Compton, photoelectron, Auger, and other secondary electrons that amplify DNA damage in cancer cells [9–11]. Among these, silver nanoparticles (AgNPs) have illustrated potential radiosensitizing and antiproliferative effects through a variety of mechanisms, such as glutathione depletion, blockage of efflux activity of drug-resistant cells, ROS generation, and apoptosis induction. Furthermore, it has been well documented that AgNPs can act as radiosensitizing agents that enhance the effects of RT [12, 13]. Nevertheless, concerns over their potential toxicity and nonspecific biodistribution have hindered the clinical translation of metal NPs.

Metformin (Met), a widely used antidiabetic drug, has recently attracted attention for its anticancer and radiosensitizing abilities [14–17]. This drug increases tumor cell sensitivity to RT by inhibiting mitochondrial complex I, disrupting cancer cell metabolism, and selectively amplifying ROS production. Additionally, preclinical studies have proposed that metformin can alleviate hypoxia in tumor cells, a known contributor factor to radioresistance, thereby improving tumor cell response to radiation [18–20]. Importantly, one of the captivating features of metformin is to protect normal tissue from oxidative damage by inhibiting endogenous ROS generation to diminish oxidative damage in healthy cells [21]. This offers a therapeutic window as an adjuvant therapy in conjunction with RT. In this regard, the radiosensitizing and anticancer potential of metformin has also been demonstrated in pancreatic, rectal, and lung cancer in recent studies [22].

The development of novel radiosensitizers may contribute to the advancement of radiation treatment. Metformin has just come to light as a potentially effective anticancer drug that can increase tumor cells' radiosensitivity [23]. Despite these advantages, its utility in clinical settings as a radiosensitizer is restricted due to its rapid systemic clearance and suboptimal tumor accumulation [24, 25].

To tackle these shortcomings, niosomes have emerged as promising nanocarrier-based drug delivery systems in the field of nanotechnology. Their unique structure, comprising an inner aqueous compartment covered by a hydrophobic membrane, enables the encapsulation of both hydrophilic and hydrophobic agents, thereby improving drug stability, bioavailability, and targeted delivery [26]. Niosomes have shown potential not only in drug delivery but also in diagnosis, monitoring, and treatment applications [27]. In this regard, encapsulating radiosensitizers such as AgNPs and metformin within niosomes offers an effective strategy to enhance the efficacy of RT by increasing the sensitivity of cancer cells to treatment while minimizing systemic toxicity.

This study proposes a novel combinational approach for lung cancer therapy by developing niosomal nanocarriers co-encapsulating metformin and silver nanoparticles (NISM@Ag-Met) as radiosensitizers in conjunction with RT. We hypothesize that this formulation could synergistically enhance the radiosensitivity of A549 lung cancer cells, resulting in greater inhibition of cell proliferation and increased apoptosis induction compared to single-agent or free-form treatments. Our work aims to address the limitations of current cancer treatment strategies and provides a novel foundation for more effective and safer lung cancer therapies.

2 | Materials and Methods

2.1 | Reagents and Materials

The Sobhan Oncology Pharmaceutical Company (Iran) provided the sorbitan monooleate (span80-CAS.1338-43-8), polyoxyethylene sorbitan monooleate (Tween 80-CAS.9005-65-6), and cholesterol (CAS.57-88-5). The Sigma-Aldrich Company (Germany) provided the chloroform reagent and 5-dimethylt hiazol-z-yl-2,5-diphenyltetrazolium bromide (MTT). Sigma-Aldrich Inc. was supplied with the $AgNO_3$ agent. Gibco, Life Technologies (NY, USA), supplied penicillin/streptomycin and Dulbecco's modified Eagle's medium (DMEM) with high glucose. PBS was used to dissolve the metformin, which was a gift from the Tehran University of Medical Sciences, and then a 0.22-μm filter was used to filter the mixture. Emertat Chimi Company (Tehran, Iran) provided all extra chemicals, solvents, and cell culture media.

2.2 | Preparation of AgNPs

AgNPs were synthesized using the Frenz technique [28]. Briefly, a magnetic stir bar was added to an Erlenmeyer flask containing 50 mL of a 1 mM $AgNO_3$ solution. The flask was heated to boiling and then covered with aluminum foil. 500 μL of sodium citrate was added dropwise after the solution reached the boiling point and stirred for 20 min. Subsequently, 2 mL of the solution was centrifuged for 30 min at 14,000 rpm, discarding the supernatant and dispersing the leftover sediment in 1 mL of distilled water. Ultimately, the mixture was then kept at 4°C in the dark.

2.3 | Preparation of Niosomes Loaded With AgNPs and Met Drug

Niosomes were prepared using the thin-film hydration method, also known as the handshaking method. Briefly, 80 mg of cholesterol and 300 mg of surfactants (Tween 80 and Span 80) were dissolved in chloroform in a round-bottom flask [29]. Chloroform was evaporated at 55°C under reduced pressure (150 rpm) using a rotary evaporator to create a thin lipid film. A 10 mL solution containing AgNPs and Met drug was added to the lipid film and vortexed vigorously for 1 min. The mixture was then sonicated for 5 min in a bath sonicator, followed by additional sonication in a 55°C water bath for 15 min to yield the final formulation, NISM@Ag-Met.

2.4 | Characterization of Synthesized NPs

Dynamic light scattering (DLS) was employed to ascertain the hydrodynamic size and its corresponding polydispersity index using a nano/zeta sizer from Malvern Instruments Ltd. The chemical structure and composition of all formulations, including NISM, and AgNPs, were characterized using Fourier transform infrared (FTIR) spectroscopy on a Bruker Tensor 27 spectrometer. To prepare samples for analysis, each formulation was thoroughly mixed with potassium bromide (KBr) at a 1:10 weight ratio. The resulting mixture was then mechanically ground and pressed into pellets under a pressure of 10 tons [30]. UV–visible (T80) spectrophotometer encompassing a wavelength range of 200–600 nm was used to perform the optical examination of NISM, NISM@Ag-Met, AgNPs, and Met drug. Field emission scanning electron microscopy (FESEM) was used to analyze the morphology and particle size of the NISM@Ag-Met utilizing an MIRA3 apparatus from TESCAN, which is based in Brno, Czech Republic. Before being analyzed using the FESEM method, the dried specimen was coated with gold [31].

2.5 | Encapsulation Efficiency (EE)

Niosomal dispersions were centrifuged at 18,000 rpm for 1 h at 4°C using a refrigerated centrifuge. Niosomal pellets were subsequently centrifuged, washed, and subjected to methanol treatment. Spectrophotometric quantification of Met was performed at a maximum wavelength of 234 nm. To determine the Met concentration, niosomes were dispersed in methanol to disrupt their structure and release the encapsulated Met [32]. Encapsulation efficiency (EE) was calculated using the following equation:

$$\text{Encapsulation efficiency (EE)}\% = \frac{\text{amount of Met encapsulated into niosomes}}{\text{amount of Met initially used}} \times 100$$

2.6 | Inductively Coupled Plasma Mass Spectrometry (ICP-MS)

A 7500ce octopole reaction system, made in California, USA, was used for the inductively coupled plasma mass spectrometry (ICP-MS) study. The objective of this investigation was to measure the concentration of total silver (Ag) following niosome breakdown.

2.7 | In Vitro Drug Release Assay

The in vitro release assays were performed under simulated physiological settings to evaluate the pH-dependent release profile of Met from the prepared NISM@Ag-Met nanocarrier. This assay was conducted in a variety of pH buffers, including pH 7.4 (which mimics intestinal fluid) and pH 5.8 (which mimics the acidic environment of cancer cell gaps), at 37°C for 72 h [33]. Pre-soaking the dialysis bags in the appropriate release medium (pH 7.4 or 5.8 PBS) for 24 h ensured full wetness and avoided any initial burst release.

After that, the dialysis bag containing 1 mL of the NISM@Ag-Met suspension was immersed in 20 mL of the corresponding release medium and kept at 37°C under gentle agitation. At predetermined time intervals, a known amount of the release medium was taken out and immediately replaced with an equivalent volume of fresh medium to keep the sink condition constant. Ultimately, using the spectrophotometry technique and standard calibration curve, the amount of Met released into the medium was measured and determined at a wavelength of 234 nm [34].

2.8 | Cell Line and Culture Conditions

Human lung cancer cell line A549 (ATCC number: CCL-185) was acquired from the Pasteur Institute of Iran's Cell Bank (Tehran, Iran). 1% penicillin–streptomycin antibiotic and 10% fetal bovine serum (FBS), both from Gibco, were added to DMEM high-glucose medium for cell growth. A humidified environment containing 5% CO_2 was used to maintain the cell culture at 37°C.

2.9 | Radiation Treatment

Using Siemens Primus-type linear accelerator equipment, x-ray irradiation was carried out at 6 MV. Samples were exposed to a radiation beam after being placed in the x-ray instrument's cabinet. The dosage rate and duration of radiation define the administered dose. In order to perform apoptosis and cell viability tests under x-ray exposure conditions, the A549 cells were seeded into the plates [35, 36]. Next, the cells were subjected to a variety of treatment regimens, such as AgNPs, Blank NISM, NISM@Ag-Met NPs, and Met at a range of concentrations (12.5, 25, 50, and 100 μg/mL) and incubated for 6 h. After removing the treatment media and adding a fresh medium to each well, the cells were exposed to 4 Gy of x-ray radiation and incubated at 37°C in 95% air and 5% CO_2.

2.10 | Cell Viability Assay

The MTT cytotoxicity test was used to evaluate the antiproliferation effects of AgNPs, Met, NISM@AgNPs, and NISM@Ag-Met against the A549 lung cancer cell line. The number of 1.2×10^4 cells per well in 96-well plates was the density at which the cells were cultured overnight at 37°C in 5% CO_2. The A549 lung cancer cells were exposed to different concentrations of the test substances after being incubated for 24 h. The media containing the synthesized NPs and Met was withdrawn after the treatment period of 6 h, and the cells were then washed with PBS. Thereafter, the cells were cultured for a further 24 h with the addition of a fresh medium. Subsequently, each well received MTT solution with a concentration of 5 mg/mL (20 μL), and following a 4-h incubation period, 100 μL of DMSO was introduced to each well. At 570 nm in wavelength, the absorbance of each sample was measured to determine the cell viability [37]. Every test was run in triplicate. For the condition that is exposed to x-ray irradiation (4 Gy, 6 MV), the same protocol is followed, with the exception that the cells are exposed to radiation after the 6-h treatment and replacement of the medium with a fresh medium [38].

2.11 | Apoptosis Assay

The initial step in evaluating apoptosis was to seed 8×10^4 A549 cells per well in 12-well plates. The samples were then subjected to a 24-h incubation period at 37°C in 5% CO_2. Following that, the cells were exposed to 50 μg/mL of AgNPs, NISM@Ag-Met NPs, and the Met. After the treatment period (6 h), the media containing NPs and drug was withdrawn, and PBS was used to wash the treated cells. The wells were then filled with fresh medium and exposed to x-ray (4 Gy, 6 MV) and incubated for 24 h. Following the manufacturer's instructions (Sigma-Aldrich), the cells were then stained with Annexin-V FITC and PI after being exposed to 100 μL of Annexin-V binding buffer [37, 39]. The analysis of the data was carried out with FlowJo software (Tree Star, Ashland, OR) and flow cytometry equipment (BD Biosciences, San Jose, CA, USA).

2.12 | Statistical Analysis

With GraphPad Prism 8 software, the data were analyzed and shown as mean ± SD (standard deviation). A statistically significant p value was defined as one that was less than 0.05. *$p < 0.05$; **$p < 0.01$; ***$p < 0.001$; and ****$p < 0.0001$. Every experiment was run in three duplicates.

3 | Results and Discussion

3.1 | Particle Size and Polydispersity Index (PDI)

Particle size and particle size distribution along with other physicochemical properties of lipidic nanocarriers influence their tendency to accumulate in the target tissue. Therefore, the development of homogeneous (monodisperse) populations of nanocarriers of a certain size is necessary for the successful formulation of efficient, safe, and stable nanocarriers. According to Figure 1A–D, the average size of NISM, AgNPs, and NISM@Ag-Met was determined by DLS, and the results showed that they were around 152.7 ± 1.069 nm, 57.16 ± 1.229, and 169.4 ± 0.8021, respectively. The polydispersity index (PDI) values for NISM, AgNPs, and NISM@Ag-Met were 0.249, 0.358 ± 0.045, and 0.413, respectively, as shown in Figure 1E. DLS size results were acceptable for cancer investigations because they were less than 200 nm in hydrodynamic size. The size findings for the AgNPs were also appropriate, as the size range is established as 1–100 nm [40, 41].

The size and PDI of the NISM@Ag-Met nanosystem were suitable for application in the treatment of cancer. These sizes coincide with the dimensions mentioned in the literature as critical to passive nanoscale targeting through an EPR effect. For example, NPs of a size close to 150 nm exert a very narrow margin and are effective in avoiding significant renal clearance yet are significantly accumulated in tumor tissues by the EPR effect [42]. As reported by Gharbavi et al., in their findings, the size of NPs for NISM@BSA and NISM-BSA@SeNPs is 118.63 ± 0.666 nm and 149.23 ± 3.164 nm, respectively [43]. Similar results were obtained by Mousazadeh et al. for methotrexate and curcumin-coencapsulated niosome NPs [44]. Another study demonstrated that monodisperse lipidic nanocarriers showed higher stability and more effective interactions with cancer cells, therefore providing better therapeutic outcomes [45].

3.2 | FTIR Analysis

As shown in Figure 2A, FTIR spectroscopy was employed to identify the functional groups present in Met, free NISM, Ag NPs, and NISM-Met-Ag NPs. The FTIR spectrum of Met exhibited a prominent absorption band at approximately 3400 cm^{-1}, characteristic of the stretching vibrations of $-NH_2$ groups. Additionally, peaks observed around 2900 and 1650 cm^{-1} were attributed to C–H stretching and C=N stretching vibrations, respectively. The spectrum of free NISM displayed a strong peak at around 3400 cm^{-1}, indicative of −OH group stretching vibrations from the NISM components. A peak near 2900 cm^{-1} was assigned to C–H stretching vibrations of alkyl chains within the niosome structure, whereas the peak at 1640 cm^{-1} corresponded to C=C stretching vibrations of unsaturated bonds in the niosome components. Previous studies have demonstrated that the characteristic absorption peaks of niosomes at 1700 cm^{-1} and 3400 cm^{-1} correspond to the presence of a carboxylic acid functional group (C=O) and a hydroxyl group, respectively [34]. The FTIR spectrum of AgNPs revealed a broad band centered around 3400 cm^{-1}, suggesting the presence of surface-bound water molecules or hydroxyl groups. Peaks around 1630 and 1380 cm^{-1} were likely due to the bending vibrations of water molecules. Furthermore, a peak at 650 cm^{-1} was observed, often associated with metal–oxygen bond stretching vibrations, potentially indicating the presence of water on the surface of the AgNPs. Mondal et al. demonstrated that the characteristic vibrational peaks of citrate-functionalized AgNPs (citrate@AgNPs) are observed at 1600 cm^{-1} (C=O stretching) and 1329 cm^{-1} (C–O stretching), along with a broad absorption band in the range of 3200–3420 cm^{-1} corresponding to O–H stretching [46], which

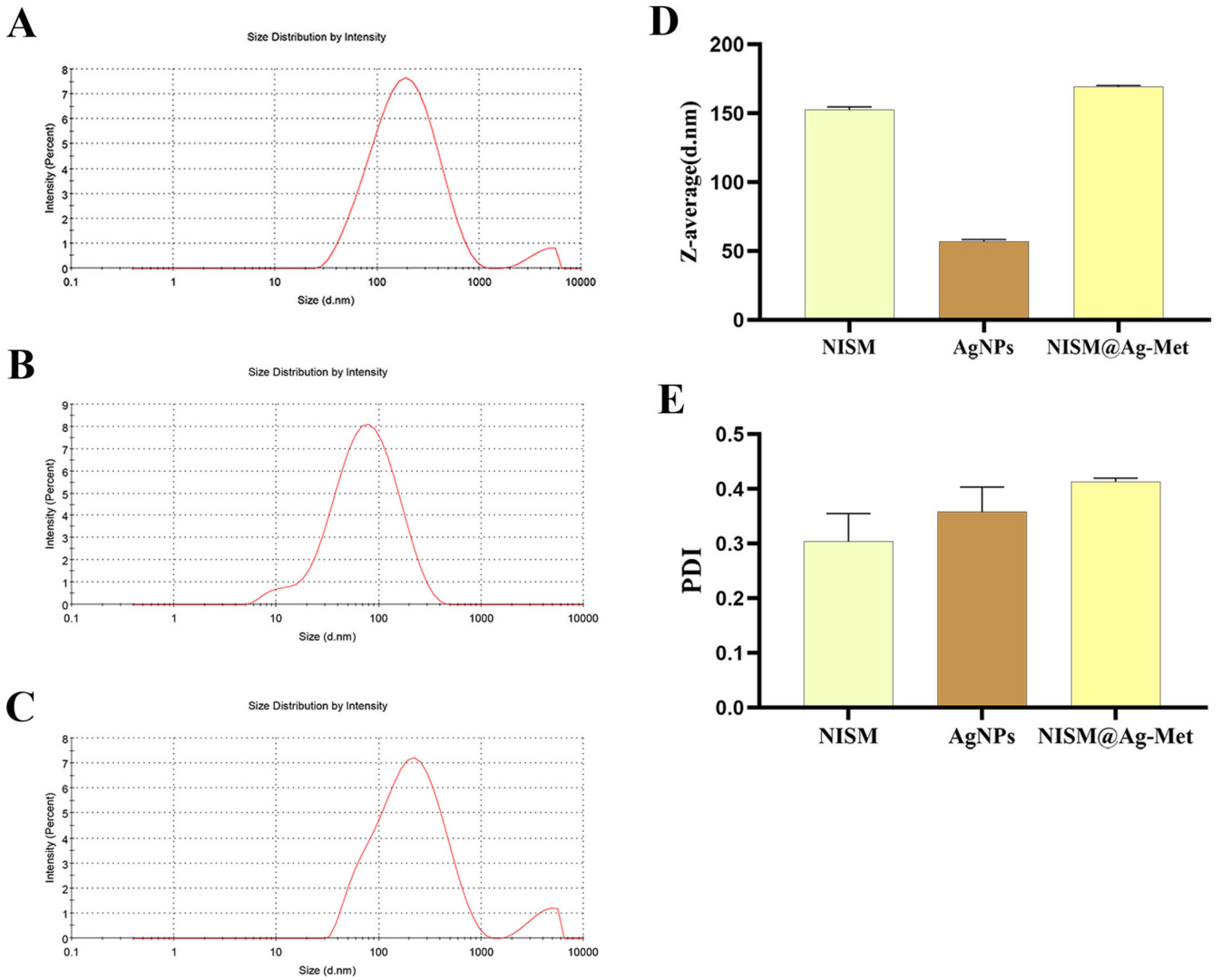

FIGURE 1 | Hydrodynamic size distribution of the synthesized nanoparticles: (A) NISM, (B) AgNPs, (C) NISM@Ag-Met, (D) analyzed data of hydrodynamic diameter, and (E) polydispersity index (PDI) for all groups.

is in line with our findings. As a result, slight changes in the peak position could depend on the different materials used to synthesize the AgNPs. The most important bands were detected through FT-IR in Begam's study at 3383, 2352, 1601, 1404, 1113, 675, and 518 cm^{-1}, whereas the band at 2352 cm^{-1} matched the O–H stretching vibration to that of the functional group carboxylic acid; also at 1601 cm^{-1}, which showed a C=C stretching match corresponding to aromatic amino groups. The band at 675 cm^{-1} is assigned to C–H stretching in the phenyl ring of substitution bands, and characteristic stretch for AgNPs was found around 518 cm^{-1} [47]. The FTIR spectrum of NISM-Met-AgNPs exhibited absorption bands characteristic of both Met and AgNPs, confirming the successful encapsulation of these components within the NISM system.

3.3 | UV–Vis Analysis

UV–Vis spectroscopy has shown to be an effective method for characterizing developed NPs. AgNPs are reported to display a 400–500 nm UV–Vis absorption due to surface plasmon resonance [48]. In this investigation, it was found that the produced AgNPs' λmax value was 439 nm. Abraham et al. confirmed the biosynthesis of AgNPs from $AgNO_3$ solution through UV–Vis spectroscopic analysis. This process was evidenced by a color change from greenish to brown, with the maximum absorbance observed at 420 nm [49]. Begam studied the biosynthesis of AgNPs using marine bacteria. The UV–Vis spectroscopy of AgNPs showed the characteristic absorption peak at 420 nm due to surface plasmon resonance [47]. A similar study was conducted by Huang et al., which reported the formation of AgNPs through the reduction of aqueous $AgNO_3$ (50 mL, 1 mM) using 0.1 g of biomass derived from *Cinnamomum camphora*. The synthesis was confirmed by a sharp absorbance peak at approximately 440 nm, indicative of surface plasmon resonance of the NPs [50]. Additionally, the study assessed the maximum UV absorption of Met and discovered that it was 232 nm, which is consistent with other findings in the literature [51]. In another study conducted by Karale et al., the UV–Vis absorption of metformin was found to be 234 nm [52]. Figure 2B shows that the λmax values of AgNPs and Met show a slight shift, indicating their successful encapsulation within the niosomes. This conclusion

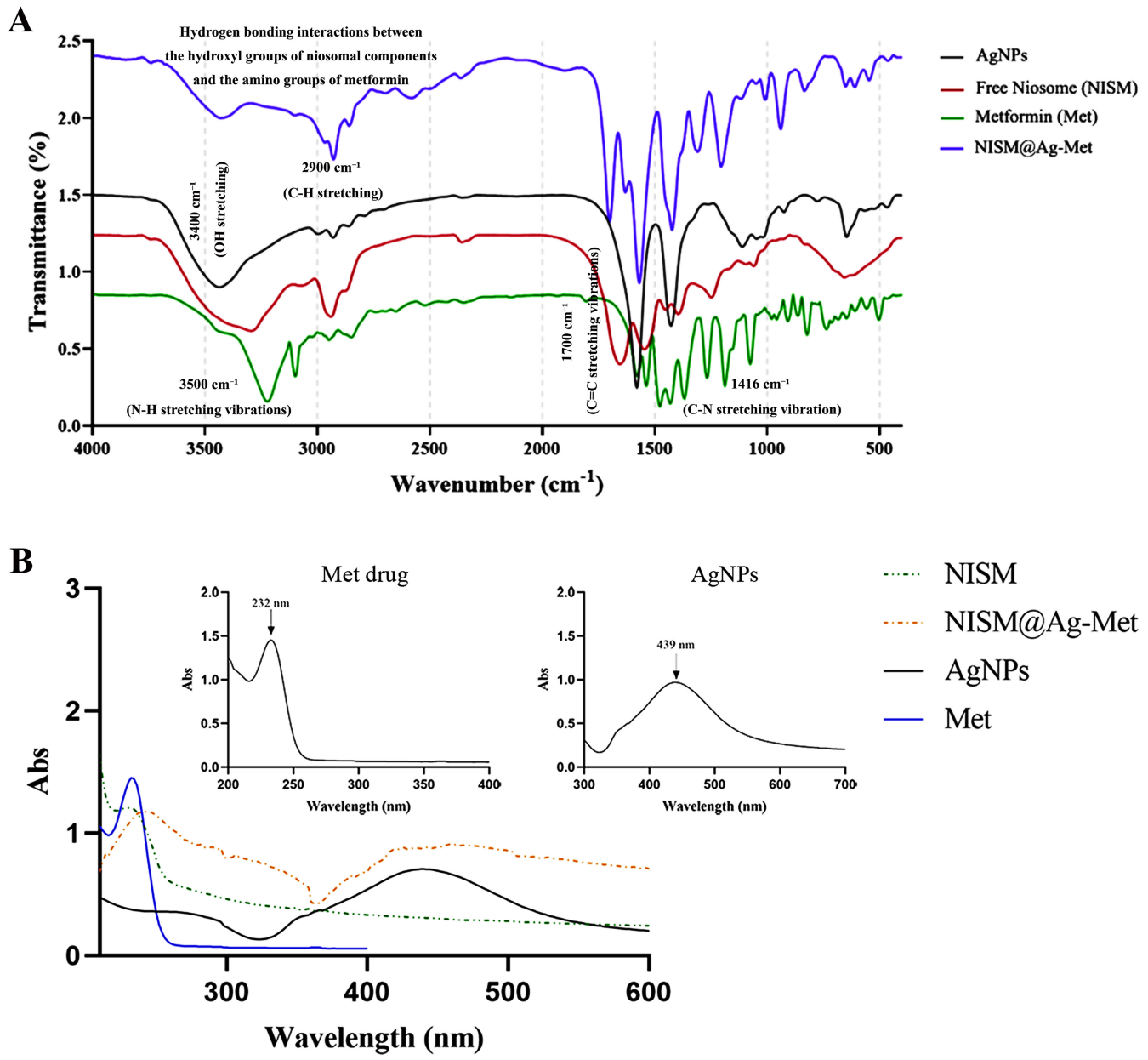

FIGURE 2 | (A) FTIR analysis (B) UV–vis absorption spectrum of NISM, NISM@Ag-Met, AgNPs, and Met drug.

is drawn from a comparison of the UV spectra of empty NISM, NISM@Ag-Met, AgNPs, and Met drug.

3.4 | Morphology of Nanoparticles

The morphology of the NPs was also examined using FESEM, and the results are shown in Figure 3A,C. The average size of NISM (Figure 3B) and NISM@Ag-Met (Figure 3D) were 31.92 ± 9.85 and 36.5 ± 8.61 nm, respectively, as evidenced by the FESEM images and their corresponding histogram of particle size distribution. These results also support the hydrodynamic size of the prepared NISM@Ag-Met, as determined by the DLS measurements. SEM images of the BSA-coated niosome formulation developed by Jafari et al. showed a homogeneous spherical morphology. The surface morphology of the niosomes was also found to be smooth, in accordance with the nature of the formulation [34].

3.5 | Encapsulation Efficiency

In this investigation, we initially assessed the absorption of Met at its λmax of 234 nm in order to assess the encapsulation effectiveness of Met within the niosomes following purification by centrifugation. The Met concentration was ascertained by utilizing the calibration curve. Also, one powerful technique for identifying and measuring AgNPs is ICP-MS. Therefore, ICP-MS was employed to ascertain the Ag content in niosomes [53, 54]. According to the findings, the percentages of encapsulation efficiency for Ag and Met were 38.56% ± 6.28% and 49.30% ± 7.89%, respectively.

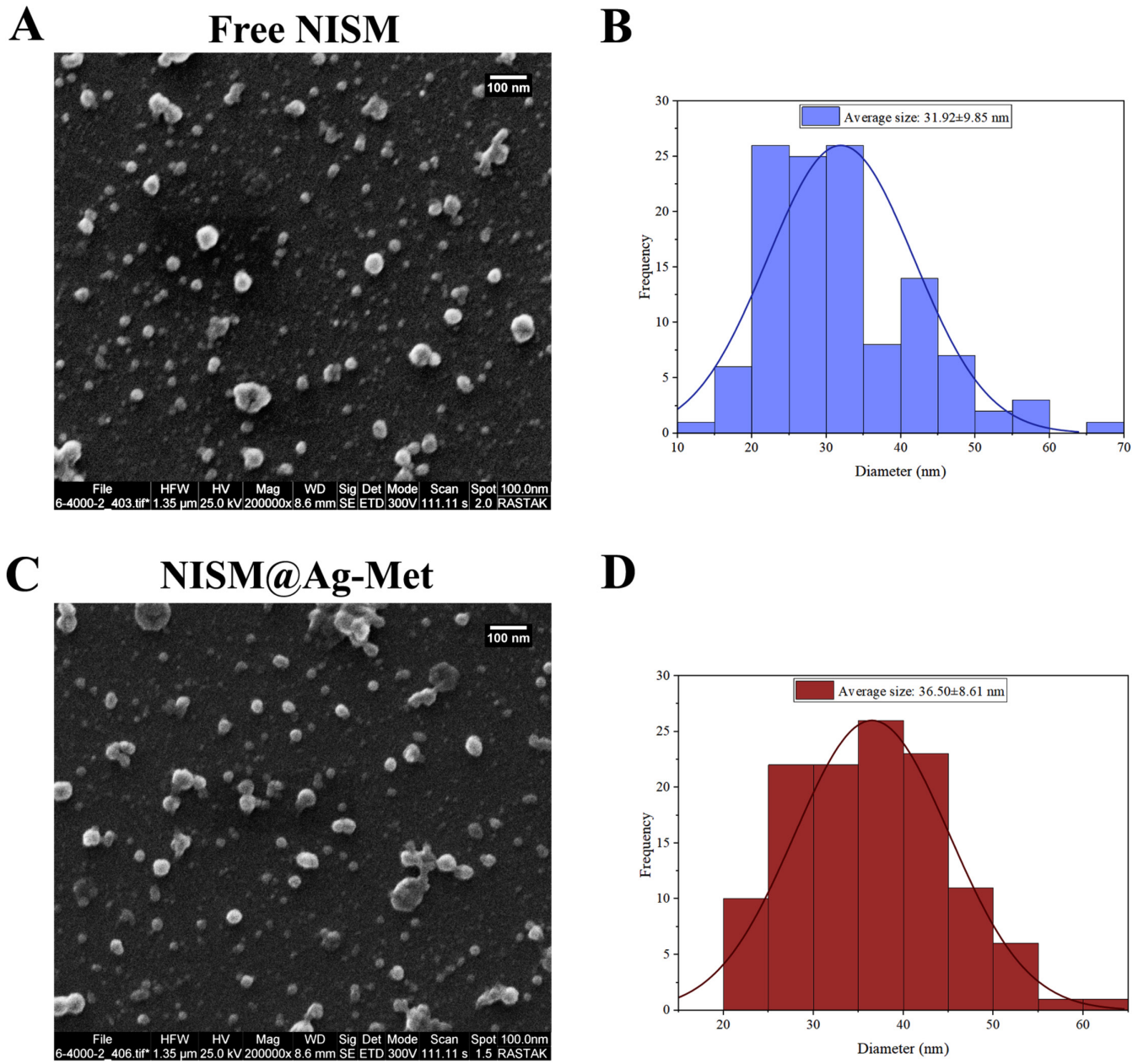

FIGURE 3 | FESEM images of (A) free NISM and (B) NISM@Ag-Met and (C, D) corresponding particle size distribution histograms.

3.6 | Drug Release Study

To evaluate the Met release profile from the NISM-Met-Ag NPs as a function of pH, in vitro release experiments were performed under simulated physiological conditions. The tests were conducted in PBS solution at two different pH levels: 5.8 (to simulate the acidic tumor microenvironment) and 7.4 (to simulate physiological settings). The temperature was maintained at 37°C for a duration of 72 h. Figure 4 illustrates the release profile of Met from the NISM-Met-Ag NPs. Figure 4 shows a burst release in the first 2 h at pH 7.4 and 5.8, followed by a continuous and sustained release throughout 3–24 h. After 72 h, a plateau phase was achieved, which indicated that the Met release was in close proximity to being completed. There was a noticeable difference in the release rate of Met between pH 5.8 and pH 7.4 from the NISM-Met-Ag NPs, indicating that the release rate was pH dependent.

The intrinsic features of the NISM nanocarriers are responsible for this pH-responsive behavior. These nanocarriers undergo structural changes in response to variations in pH.

3.7 | Cell Viability Assay With and Without Radiation Exposure

The MTT assay was performed to evaluate the cytotoxicity of blank niosomes (NISM), AgNPs, Met, and NISM@Ag-Met at concentrations of 12.5, 25, 50, and 100 µg/mL on A549 cancer cells (Figure 5A,B). The results provided good insight into the synergistic effect of combination treatments under x-ray exposure conditions.

In the without x-ray exposure condition (Figure 5A), the viability of A549 cells was remarkably different according to treatment and

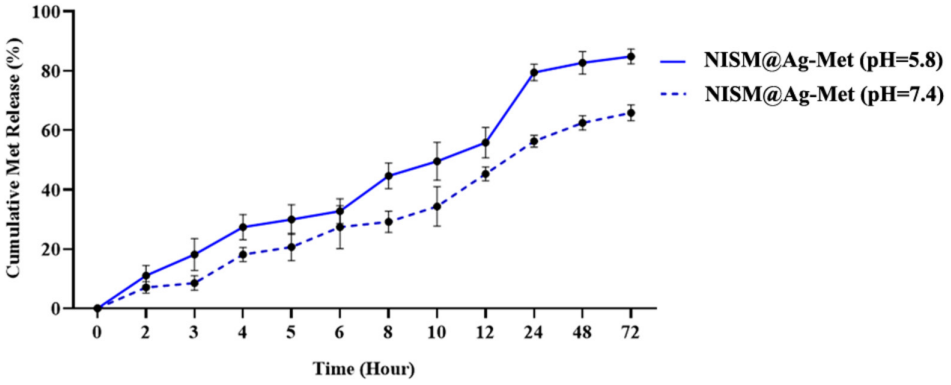

FIGURE 4 | The in vitro release profile demonstrates the pH-responsive behavior of NISM@Ag-Met nanocarriers, with accelerated drug release under acidic conditions (pH 5.8) compared to physiological pH (7.4).

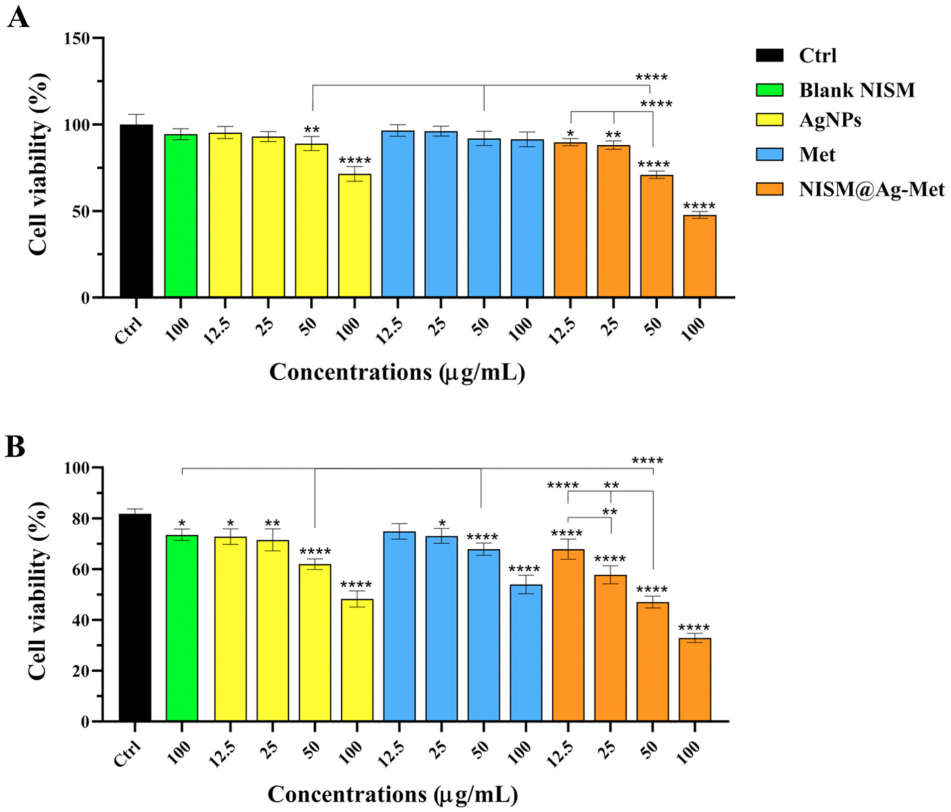

FIGURE 5 | The inhibitory effect of Met, AgNPs, and NISM@Ag-Met with different concentrations (12.5, 25, 50, and 100 μg/mL) (A) without x-irradiation and (B) with x-irradiation conditions on cell viability of A549 cells. One-way ANOVA was used for analysis. *$p < 0.05$, **$p < 0.01$, and ****$p < 0.0001$.

concentration. The cell viability was above 85% for all concentrations of the blank niosomes (NISM), which showed very low cytotoxicity. This means the toxicity of the blank NISM is negligible, and it is biocompatible. These results confirm that any observed cytotoxic effects can be attributed to the active components rather than the niosome formulation. Treatment with AgNPs showed a dose-dependent loss in cell viability. Although the reduction in viability at 12.5 μg/mL was slight, a sharp decline was seen as the concentration increased to 100 μg/mL, where cell viability fell to about 40%. This indicated that AgNPs exhibit intrinsic cytotoxic effects due to their capability of induction of oxidative stress and interference with cellular processes. Metformin alone revealed a mild cytotoxic effect, with cell viability of about 70% even at the highest concentration (100 μg/mL). This further points toward the moderate anticancer activity that has been ascribed to metformin, thus validating its reported role in inhibiting the proliferation of cancer cells through the activation of AMPK and mitochondrial dysfunction. NISM@Ag-Met presented the highest cytotoxic effect among treatments, showing cell viability of around 60% at a low concentration of 12.5 μg/mL and decreased below 20% at 100 μg/mL. This highly improved cytotoxicity emphasizes the synergistic effect of using AgNPs and metformin together in a niosome formulation. In such a formulation, the bioavailability and delivery at the target site would be enhanced, hence increasing its efficacy.

Under x-ray exposure conditions (Figure 5B), the blank niosomes maintained high cell viability across all concentrations, reinforcing their biocompatibility and lack of inherent cytotoxicity even under x-irradiation. Under x-ray exposure conditions, high cell viability was maintained across all concentrations by the blank niosomes (NISM), further confirming their biocompatibility and absence of inherent cytotoxicity even under x-ray exposure. A significant enhancement in the cytotoxicity of AgNPs was observed in the presence of x-irradiation. Cell viability was recorded at approximately 60% at 12.5 μg/mL, decreasing to below 20% at the highest concentration of 100 μg/mL. This increased cytotoxicity is likely attributed to the radiosensitizing effect of AgNPs, which is associated with their ability to generate ROS under radiation exposure. Increased cytotoxic effects were exhibited by metformin when combined with radiotherapy, with cell viability reducing to approximately 50% at 100 μg/mL. This enhancement aligns with metformin's role in improving radiotherapy efficacy by alleviating hypoxia and sensitizing cells to damage induced by radiation. The most pronounced reduction in cell viability under x-irradiation conditions was observed with the NISM@Ag-Met formulation, with viability decreasing to below 10% at concentrations of 50 μg/mL and higher. This striking result highlights the potent synergistic effect of the combination therapy, with substantial cytotoxicity induced by the combined action of the radiosensitizing properties of AgNPs and the metabolic disruption caused by metformin. The retention and stability of the active agents are likely enhanced by the niosome encapsulation, further amplifying their therapeutic potential.

The data clearly show that the cytotoxic effects of all treatments are significantly enhanced by radiotherapy, with the effects being most pronounced in those involving AgNPs and NISM@Ag-Met. The NISM@Ag-Met formulation was consistently found to outperform the individual treatments, both in the presence and absence of x-ray exposure. These findings emphasize the potential of NISM@Ag-Met as a promising candidate for combined chemoradiotherapy in the treatment of lung cancer.

It was reported by Guo et al. that green-synthesized AgNPs exhibited significant anticancer activity, with cell viability in pancreatic cancer models being reduced through the induction of oxidative stress and mitochondrial damage [55]. These findings align with the observations of AgNP-induced cytotoxicity in A549 cells, particularly at higher concentrations. It was demonstrated by Karuppiah et al. that biogenically synthesized AgNPs, when combined with anticancer drugs, significantly enhanced cytotoxic effects in breast cancer cell lines, emphasizing the potential of AgNPs in combination therapies [56]. It was highlighted by Liu et al. that AgNPs amplify radiation-induced cell death through the generation of ROS [57]. Additionally, it was demonstrated by Jang et al. that the combination of metformin with AKT inhibitors significantly increased its cytotoxic effects in NSCLC cells and enhanced their sensitivity to RT [58]. Similarly, metformin's activation of AMPK and inhibition of mTOR were highlighted by Singh-Makkar et al. as key mechanisms underlying its anticancer effects [59]. In addition, a study reported that the proliferation of MCF-7 and A549 cells is inhibited by metformin and gold NPs in a dose- and time-dependent manner [60].

3.8 | Apoptosis Assay With and Without Radiation Exposure

The apoptosis assay was performed on A549 cancer cells under different treatment conditions, including metformin (Met), AgNPs, and NISM@Ag-Met, with and without x-irradiation. Under no x-ray exposure condition (Figure 6A,C), the apoptosis rates are quite different among the treatment groups. Met drug induced a modest increase in apoptosis compared to the control, consistent with its reported metabolic stress effects on cancer cells. Cytotoxicity of AgNPs is manifested, probably through the induction of oxidative stress and interference with cellular functions, as a more pronounced rate of apoptosis. However, NISM@Ag-Met results in the highest degree of apoptosis, showing that there is a synergistic effect when metformin is delivered with AgNPs. This synergy could potentiate the pathways of oxidative and metabolic stress, amplifying apoptosis.

When the x-ray exposure condition is applied, as in Figure 6B,D, the rate of apoptosis increases in each group. X-irradiation alone usually induces DNA damage, which then leads to apoptosis, but its combination with chemical treatments reveals striking trends. In this, the control group has a minute increase in apoptosis due to the x-irradiation effect. Similarly, the Met drug treatment increases apoptosis slightly, at least by interfering with metabolic pathways and sensitizing cell populations to radiation-induced injury. It also confirms that AgNPs are radiosensitizers and induce a significant increase of apoptosis upon x-irradiation, thus exacerbating oxidative stress. Indeed, the highest value of apoptosis was found for the treatment with NISM@Ag-Met, far beyond those from other treatments. This result underlines the enhanced therapeutic efficacy of the combined nanosystem under x-ray exposure conditions, probably due to targeted delivery, improved bioavailability, and the dual-action mechanisms of metabolic disruption and oxidative damage.

It has been documented that Met causes an increase in the apoptosis rate of A549 cells [61, 62]. However, another research shows that Met causes A549 lung cancer cells to undergo apoptosis via influencing ROS levels, changing the bax/bcl-2 ratio, and modifying the expression of the p-AMPK protein [62]. Furthermore, studies have demonstrated that Met causes apoptosis in A549 cells and makes NSCLC cells more susceptible to celecoxib-induced apoptosis [63]. These findings, which showed that Met might raise the radiosensitivity of NSCLC cells by disrupting NRF2, were also published by Sun et al., which is completely consistent with our findings [22]. AgNPs have demonstrated substantial apoptotic activity in A549 cells across several studies. The potent radiosensitizing ability of AgNPs against different cancer types has been extensively reported. Ghaffarlou et al. prepared AgNPs through facile biomineralization methods and assessed their radiosensitization capability against breast cancer. Both in vivo and in vitro results confirmed the radio-enhancing ability of developed NPs [64]. Overall, the enhanced incidence of apoptosis seen in cells treated with NISM@Ag-Met following x-ray exposure is likely caused by the inclusion of both Met and AgNPs in the structure of produced NPs, which operate as potent radiosensitizers.

Although AgNPs are highly effective as radiosensitizers, their potential long-term cytotoxic and oxidative stress effects on healthy

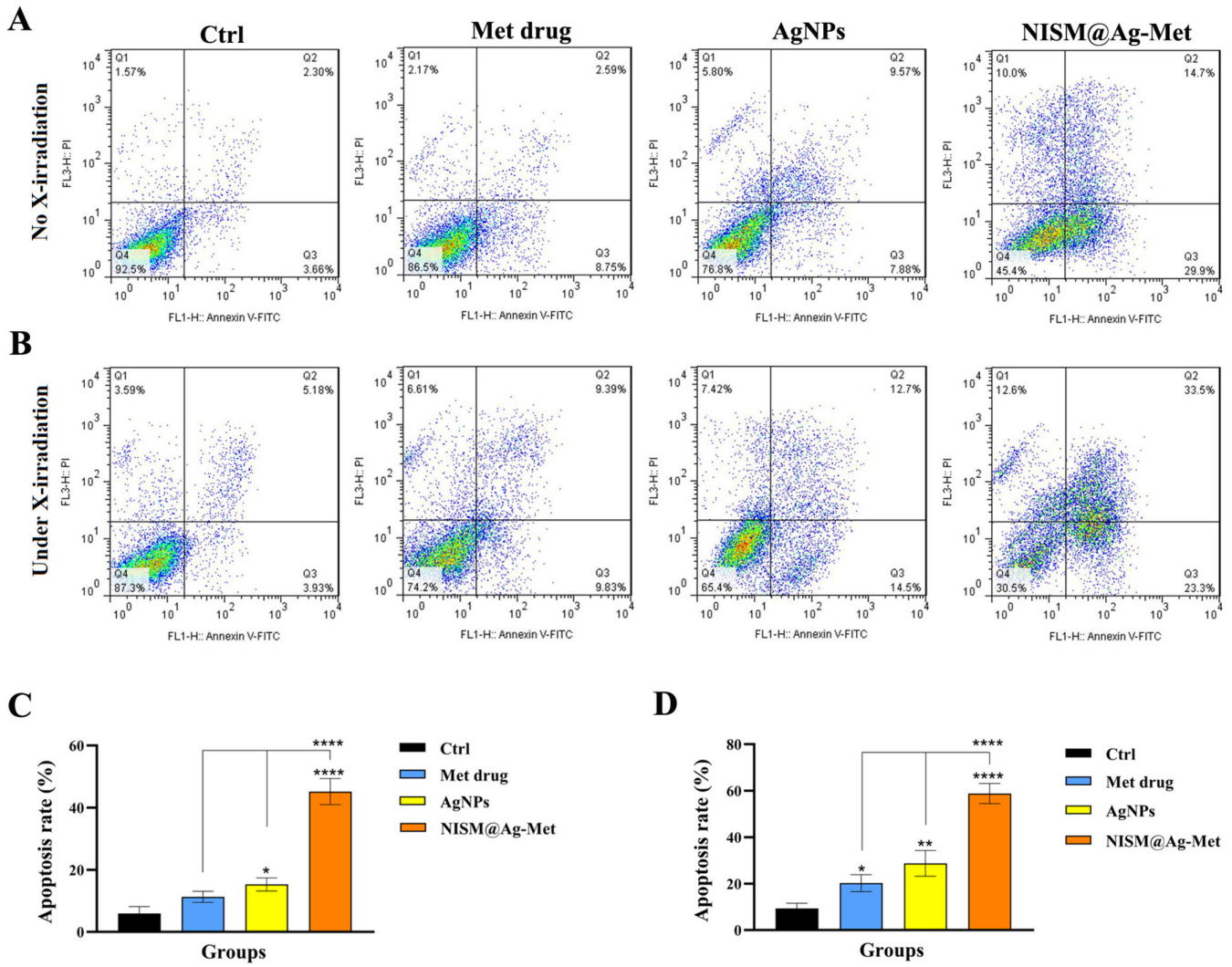

FIGURE 6 | Apoptosis rate of A549 lung cancer cells treated by Met, AgNPs, and NISM@Ag-Met under (A,C) without x-irradiation and (B,D) with x-irradiation conditions. In the flowcharts of apoptosis analysis: fluorescence intensity for Annexin V/FITC is plotted on the x-axis, and PI is plotted on the y-axis (Q1, necrosis; Q2, late apoptosis; Q3, early apoptosis; Q4, live cells). One-way ANOVA was used for analysis. $^{*}p < 0.05$, $^{**}p < 0.01$, and $^{****}p < 0.0001$.

tissues highlight the need for careful dose optimization and thorough toxicity profiling [65, 66]. A significant challenge on NISM@Ag-Met delivery is achieving precise and controlled release in vivo, given the variability of tumor microenvironments across individuals. Future studies should explore functionalizing NISM surfaces with ligands to enhance targeted delivery and assess immune responses. Functionalizing NISM—such as with folate or peptides targeting EGFR and CD44—can enable active targeting of lung cancer cells, enhancing their therapeutic potential [67].

4 | Conclusion

The current study demonstrates that the preparation of niosomes containing radiosensitizing compounds, such as AgNPs and Met, can enhance lung cancer suppression and improve therapeutic efficacy when used in conjunction with RT. The MTT assay results revealed that the engineered NISM@Ag-Met NPs exhibited significantly higher cytotoxic effects on cell viability compared to other treatment groups following x-irradiation. This suggests that the combination of NISM@Ag-Met NPs with x-ray exposure can effectively inhibit the cell growth of lung cancer cells. Furthermore, x-irradiation in combination with NISM@Ag-Met NPs markedly induced apoptosis in the A549 lung cancer cell line, corroborating the findings from the MTT assay. Overall, the in vitro results indicate that the developed nanoplatforms (NISM@Ag-Met) possess a high potential for radiosensitization and can efficiently suppress lung tumor cells. To fully realize their potential in clinical settings, extensive investigations across various cancer cell lines are warranted, followed by comprehensive in vivo assessments.

Author Contributions

Hamid Rashidzadeh: methodology, software, review and editing. **Mahmoud Gharbavi:** methodology, software, review and editing. **Roghayeh Ghorbani:** methodology, writing – original draft. **Mahdis Nazari:** methodology. **Hadi Noei:** software, writing – original draft. **Behrooz Johari:** supervision, conceptualization, project administration, writing – review and editing, final approval.

Acknowledgments

We are grateful to the Medical Biotechnology Department of Zanjan University of Medical Sciences and Zanjan Pharmaceutical Biotechnology Research Center for their technical assistance.

Conflicts of Interest

The authors declare no conflicts of interest.

Data Availability Statement

The data sets used and/or analyzed during the current study are available from the corresponding author on a reasonable request.

References

1. H. Sung, J. Ferlay, R. L. Siegel, et al., "Global Cancer Statistics 2020: GLOBOCAN Estimates of Incidence and Mortality Worldwide for 36 Cancers in 185 Countries," *CA: A Cancer Journal for Clinicians* 71, no. 3 (2021): 209–249.

2. C. Zappa and S. A. Mousa, "Non-Small Cell Lung Cancer: Current Treatment and Future Advances," *Translational Lung Cancer Research* 5, no. 3 (2016): 288–300.

3. C. M. Rudin, E. Brambilla, C. Faivre-Finn, and J. Sage, "Small-Cell Lung Cancer," *Nature Reviews. Disease Primers* 7, no. 1 (2021): 3.

4. C. Gridelli, A. Rossi, D. P. Carbone, et al., "Non-Small-Cell Lung Cancer," *Nature Reviews Disease Primers* 1, no. 1 (2015): 15009.

5. P. P. Connell and S. Hellman, "Advances in Radiotherapy and Implications for the Next Century: A Historical Perspective," *Cancer Research* 69, no. 2 (2009): 383–392.

6. R. Baskar, J. Dai, N. Wenlong, R. Yeo, and K. W. Yeoh, "Biological Response of Cancer Cells to Radiation Treatment," *Frontiers in Molecular Biosciences* 1 (2014): 24.

7. F. Boateng and W. Ngwa, "Delivery of Nanoparticle-Based Radiosensitizers for Radiotherapy Applications," *International Journal of Molecular Sciences* 21, no. 1 (2019): 273.

8. H. Wang, X. Mu, H. He, and X.-D. Zhang, "Cancer Radiosensitizers," *Trends in Pharmacological Sciences* 39, no. 1 (2018): 24–48.

9. M. Babaei and M. Ganjalikhani, "The Potential Effectiveness of Nanoparticles as Radio Sensitizers for Radiotherapy," *BioImpacts* 4, no. 1 (2014): 15–20.

10. S. Her, D. A. Jaffray, and C. Allen, "Gold Nanoparticles for Applications in Cancer Radiotherapy: Mechanisms and Recent Advancements," *Advanced Drug Delivery Reviews* 109 (2017): 84–101.

11. L. Gong, Y. Zhang, C. Liu, M. Zhang, and S. Han, "Application of Radiosensitizers in Cancer Radiotherapy," *International Journal of Nanomedicine* 16 (2021): 1083–1102.

12. Y. Liu, P. Zhang, F. Li, et al., "Metal-Based Nanoenhancers for Future Radiotherapy: Radiosensitizing and Synergistic Effects on Tumor Cells," *Theranostics* 8, no. 7 (2018): 1824–1849.

13. N. Mousazadeh, F. Seidi, M. Ghaffarlou, et al., "Silver Sulfide Coated Alginate Radioenhancer for Enhanced X-Ray Radiation Therapy of Breast Cancer," *International Journal of Biological Macromolecules* 234 (2023): 123636.

14. A. Vazquez-Martin, C. Oliveras-Ferraros, S. Del Barco, B. Martin-Castillo, and J. A. Menendez, "The Anti-Diabetic Drug Metformin Suppresses Self-Renewal and Proliferation of Trastuzumab-Resistant Tumor-Initiating Breast Cancer Stem Cells," *Breast Cancer Research and Treatment* 126 (2011): 355–364.

15. N. P. Nguyen, F. S. Almeida, A. Chi, et al., "Molecular Biology of Breast Cancer Stem Cells: Potential Clinical Applications," *Cancer Treatment Reviews* 36, no. 6 (2010): 485–491.

16. H. A. Hirsch, D. Iliopoulos, P. N. Tsichlis, and K. Struhl, "Metformin Selectively Targets Cancer Stem Cells, and Acts Together With Chemotherapy to Block Tumor Growth and Prolong Remission," *Cancer Research* 69, no. 19 (2009): 7507–7511.

17. R. Rattan, R. Ali Fehmi, and A. Munkarah, "Metformin: An Emerging New Therapeutic Option for Targeting Cancer Stem Cells and Metastasis," *Journal of Oncology* 2012, no. 1 (2012): 928127.

18. C. W. Song, H. Lee, R. P. Dings, et al., "Metformin Kills and Radiosensitizes Cancer Cells and Preferentially Kills Cancer Stem Cells," *Scientific Reports* 2, no. 1 (2012): 362.

19. H. D. Skinner, M. R. McCurdy, A. E. Echeverria, et al., "Metformin Use and Improved Response to Therapy in Esophageal Adenocarcinoma," *Acta Oncologica* 52, no. 5 (2013): 1002–1009.

20. S. L. Brown, A. Kolozsvary, D. M. Isrow, et al., "A Novel Mechanism of High Dose Radiation Sensitization by Metformin," *Frontiers in Oncology* 9 (2019): 247.

21. A. T. Agbele, O. P. Faromika, O. O. Awe, F. R. Amodu, G. O. Edaogbogun, and K. A. Bello, "Impact of Metformin on the Therapeutic Effect of Radiotherapy," *Radiation Medicine and Protection* 2, no. 1 (2021): 17–22.

22. X. Sun, M. Dong, Y. Gao, et al., "Metformin Increases the Radiosensitivity of Non-Small Cell Lung Cancer Cells by Destabilizing NRF2," *Biochemical Pharmacology* 199 (2022): 114981.

23. T. Deguchi, K. Hosoya, S. Kim, et al., "Metformin Preferentially Enhances the Radio-Sensitivity of Cancer Stem-Like Cells With Highly Mitochondrial Respiration Ability in HMPOS," *Molecular Therapy* 22 (2021): 143–151.

24. A. Mogavero, M. V. Maiorana, S. Zanutto, et al., "Metformin Transiently Inhibits Colorectal Cancer Cell Proliferation as a Result of Either AMPK Activation or Increased ROS Production," *Scientific Reports* 7, no. 1 (2017): 15992.

25. B. Farhood, M. Najafi, E. Salehi, et al., "Disruption of the Redox Balance With Either Oxidative or Anti-Oxidative Overloading as a Promising Target for Cancer Therapy," *Journal of Cellular Biochemistry* 120, no. 1 (2019): 71–76.

26. K. M. Kazi, A. S. Mandal, N. Biswas, et al., "Niosome: A Future of Targeted Drug Delivery Systems," *Journal of Advanced Pharmaceutical Technology & Research* 1, no. 4 (2010): 374–380.

27. M. Masjedi and T. Montahaei, "An Illustrated Review on Nonionic Surfactant Vesicles (Niosomes) as an Approach in Modern Drug Delivery: Fabrication, Characterization, Pharmaceutical, and Cosmetic Applications," *Journal of Drug Delivery Science and Technology* 61 (2021): 102234.

28. M. Gakiya-Teruya, L. Palomino-Marcelo, and J. C. F. Rodriguez-Reyes, "Synthesis of Highly Concentrated Suspensions of Silver Nanoparticles by Two Versions of the Chemical Reduction Method," *Methods and Protocols* 2, no. 1 (2018): 3.

29. M. Gharbavi, S. Parvanian, M. P. Leilan, S. Tavangar, M. Parchianlou, and A. Sharafi, "Niosomes-Based Drug Delivery in Targeting the Brain Tumors Via Nasal Delivery," in *Nasal Drug Delivery: Formulations, Developments, Challenges, and Solutions* (Springer International Publishing, 2023): 279–324.

30. H. Felenji, B. Johari, M. Moradi, M. Gharbavi, and H. Danafar, "Folic Acid-Conjugated Iron Oxide Magnetic Nanoparticles Based on Bovine Serum Albumin (BSA) for Targeted Delivery of Curcumin to Suppress Liver Cancer Cells," *Chemistry Africa* 5, no. 5 (2022): 1627–1639.

31. M. Gharbavi, B. Johari, R. M. Tabar, and A. Sharafi, "Selenium-Doped Albumin Nanoparticles Enhance Tamoxifen-Induced Anticancer Effects in 4T-1 Mouse Breast Cancer Cells," *Applied Organometallic Chemistry* 38, no. 2 (2024): e7327.

32. B. Johari, M. P. Leilan, M. Gharbavi, Y. Mortazavi, A. Sharafi, and H. Rezaeejam, "Combinational Therapy With Myc Decoy

Oligodeoxynucleotides Encapsulated in Nanocarrier and X-Irradiation on Breast Cancer Cells," *Oncology Research* 32, no. 2 (2024): 309–323.

33. B. Johari, S. Tavangar-Roosta, M. Gharbavi, A. Sharafi, S. Kaboli, and H. Rezaeejam, "Suppress the Cell Growth of Cancer Stem-Like Cells (NTERA-2) Using Sox2-Oct4 Decoy Oligodeoxynucleotide–Encapsulated Niosomes-Zinc Hybrid Nanocarriers Under X-Irradiation," *Heliyon* 10, no. 13 (2024): e34096.

34. B. Jafari, M. Gharbavi, Y. Baghdadchi, et al., "Mitigated Oxidative Stress and Cognitive Impairments in Transient Global Ischemia Using Niosomal Selegiline-NBP Delivery," *Behavioural Neurology* 2022, no. 1 (2022): 4825472.

35. R. Ghorbani, M. Gharbavi, A. Sharafi, et al., "Targeted Anti-Tumor Synergistic Effects of Myc Decoy Oligodeoxynucleotides-Loaded Selenium Nanostructure Combined With Chemoradiotherapy on LNCaP Prostate Cancer Cells," *Oncology Research* 32, no. 1 (2024): 101–125.

36. H. Soroushnasab, M. Gharbavi, M. Eskandari, H. Rezaeejam, R. Ghorbani, and B. Johari, "Methotrexate-Conjugated Silver Nanoparticles Enhance Chemoradiotherapy Effects on U87 Human Glioblastoma Multiforme Cells: As a Radiosensitizer Agent to Enhance X-Irradiation Efficacy," *Journal of Drug Delivery Science and Technology* 107 (2025): 106791.

37. N. Asadi, M. Gharbavi, H. Rezaeejam, A. Farajollahi, and B. Johari, "Zinc Nanoparticles Coated With Doxorubicin-Conjugated Alginate as a Radiation Sensitizer in Triple-Negative Breast Cancer Cells," *International Journal of Pharmaceutics* 659 (2024): 124285.

38. M. Rahmati, B. Johari, M. Kadivar, E. Rismani, and Y. Mortazavi, "Suppressing the Metastatic Properties of the Breast Cancer Cells Using STAT3 Decoy Oligodeoxynucleotides: A Promising Approach for Eradication of Cancer Cells by Differentiation Therapy," *Journal of Cellular Physiology* 235, no. 6 (2020): 5429–5444.

39. R. Ghorbani, M. Gharbavi, B. Keshavarz, H. Madanchi, and B. Johari, "Targeting c-Myc With Decoy Oligodeoxynucleotide-Loaded Polycationic Nanoparticles Inhibits Cell Growth and Induces Apoptosis in Cancer Stem-Like Cells (NTERA-2)," *Molecular Biology Reports* 51, no. 1 (2024): 623.

40. S. P. Dubey, M. Lahtinen, and M. Sillanpää, "Tansy Fruit Mediated Greener Synthesis of Silver and Gold Nanoparticles," *Process Biochemistry* 45, no. 7 (2010): 1065–1071.

41. L. M. Fu, J. H. Hsu, M. K. Shih, et al., "Process Optimization of Silver Nanoparticle Synthesis and Its Application in Mercury Detection," *Micromachines (Basel)* 12, no. 9 (2021): 1123.

42. B. Layek, B. Gidwani, S. Tiwari, V. Joshi, V. Jain, and A. Vyas, "Recent Advances in Lipid-Based Nanodrug Delivery Systems in Cancer Therapy," *Current Pharmaceutical Design* 26, no. 27 (2020): 3218–3233.

43. M. Gharbavi, B. Johari, N. Mousazadeh, et al., "Hybrid of Niosomes and Bio-Synthesized Selenium Nanoparticles as a Novel Approach in Drug Delivery for Cancer Treatment," *Molecular Biology Reports* 47 (2020): 6517–6529.

44. N. Mousazadeh, M. Gharbavi, H. Rashidzadeh, H. Nosrati, H. Danafar, and B. Johari, "Anticancer Evaluation of Methotrexate and Curcumin-Coencapsulated Niosomes Against Colorectal Cancer Cell Lines," *Nanomedicine* 17, no. 4 (2022): 201–217.

45. P. Graván, A. Aguilera-Garrido, J. A. Marchal, S. A. Navarro-Marchal, and F. Galisteo-González, "Lipid-Core Nanoparticles: Classification, Preparation Methods, Routes of Administration and Recent Advances in Cancer Treatment," *Advances in Colloid and Interface Science* 314 (2023): 102871.

46. P. Mondal and J. L. Yarger, "Synthesis and Characterization of 1 H-Imidazole-4,5-Dicarboxylic Acid-Functionalized Silver Nanoparticles: Dual Colorimetric Sensors of Zn^{2+} and Homocysteine," *ACS Omega* 7, no. 37 (2022): 33423–33431.

47. J. N. Begam, "Biosynthesis and Characterization of Silver Nanoparticles (AgNPs) Using Marine Bacteria Against Certain Human Pathogens," *International Journal of Advances in Scientific Research* 2, no. 7 (2016): 152–156.

48. M. Sastry, K. S. Mayya, and K. Bandyopadhyay, "pH Dependent Changes in the Optical Properties of Carboxylic Acid Derivatized Silver Colloidal Particles," *Colloids and Surfaces A: Physicochemical and Engineering Aspects* 127, no. 1–3 (1997): 221–228.

49. J. Abraham, S. Saraf, V. Mustafa, Y. Chaudhary, and S. Sivanangam, "Synthesis and Evaluation of Silver Nanoparticles Using *Cymodocea rotundata* Against Clinical Pathogens and Human Osteosarcoma Cell Line," *Journal of Applied Pharmaceutical Science* 7, no. 6 (2017): 55–61.

50. J. Huang, Q. Li, D. Sun, et al., "Biosynthesis of Silver and Gold Nanoparticles by Novel Sundried *Cinnamomum camphora* Leaf," *Nanotechnology* 18, no. 10 (2007): 105104.

51. S. Mandadi and M. Venkataswamy, "Formulation and Evaluation of Metformin Transcutaneous Patches," (2018).

52. K. A. Ashok, A. A. Wahid, and A. Ashok, "Formulation, Development and Absorption Enhancement of Metformin Hydrochloride by Using Spray Drying Technique," *World Journal of Pharmaceutical Research* 5, no. 4 (2015): 1671–1693.

53. M. V. Taboada-López, D. Bartczak, S. Cuello-Núñez, H. Goenaga-Infante, P. Bermejo-Barrera, and A. Moreda-Piñeiro, "AF4-UV-ICP-MS for Detection and Quantification of Silver Nanoparticles in Seafood After Enzymatic Hydrolysis," *Talanta* 232 (2021): 122504.

54. R. J. Peters, Z. H. Rivera, G. van Bemmel, H. J. Marvin, S. Weigel, and H. Bouwmeester, "Development and Validation of Single Particle ICP-MS for Sizing and Quantitative Determination of Nano-Silver in Chicken Meat," *Analytical and Bioanalytical Chemistry* 406 (2014): 3875–3885.

55. J. Guo, Y. Li, Z. Yu, et al., "Novel Green Synthesis and Characterization of a Chemotherapeutic Supplement by Silver Nanoparticles Containing *Berberis thunbergii* Leaf for the Treatment of Human Pancreatic Cancer," *Biotechnology and Applied Biochemistry* 69, no. 3 (2022): 887–897.

56. A. Karuppaiah, R. Rajan, M. Ramanathan, and A. Nagarajan, "Cytotoxicity and Synergistic Effect of Biogenically Synthesized Ternary Therapeutic Nano Conjugates Comprising Plant Active Principle, Silver and Anticancer Drug on MDA-MB-453 Breast Cancer Cell Line," *Asian Pacific Journal of Cancer Prevention: APJCP* 21, no. 1 (2020): 195.

57. P. Liu, Z. Huang, Z. Chen, et al., "Silver Nanoparticles: A Novel Radiation Sensitizer for Glioma?," *Nanoscale* 5, no. 23 (2013): 11829–11836.

58. S.-k. Jang, S. E. Hong, D. H. Lee, et al., "Inhibition of AKT Enhances the Sensitivity of NSCLC Cells to Metformin," *Anticancer Research* 41, no. 7 (2021): 3481–3487.

59. S. Singh-Makkar, K. Pandav, D. Hathaway, III, T. Paul, and P. Youssef, "Multidimensional Mechanisms of Metformin in Cancer Treatment," *Tumori Journal* 108, no. 2 (2022): 111–118.

60. A. Yeşildağ, H. T. Kızıloğlu, E. Dirican, E. Erbaş, V. Gelen, and A. Kara, "Anticarcinogenic Effects of Gold Nanoparticles and Metformin Against MCF-7 and A549 Cells," *Biological Trace Element Research* 202, no. 10 (2024): 4494–4507.

61. N. Wu, C. Gu, H. Gu, H. Hu, Y. Han, and Q. Li, "Metformin Induces Apoptosis of Lung Cancer Cells Through Activating JNK/p38 MAPK Pathway and GADD153," *Neoplasma* 58, no. 6 (2011): 482–490.

62. Z. Yu, F. Liu, and X. J. T. J.o. P. R. Zhang, "Metformin Promotes Apoptosis of A549 Cells via Regulation of P-AMPK Protein Expression, Bax/bcl-2 Ratio and ROS Levels," *Tropical Journal of Pharmaceutical Research* 20, no. 9 (2021): 1827–1832.

63. N. Cao, Y. Lu, J. Liu, et al., "Metformin Synergistically Enhanced the Antitumor Activity of Celecoxib in Human Non-Small Cell Lung Cancer Cells," *Frontiers in Pharmacology* 11 (2020): 1094.

64. M. Ghaffarlou, A. Mohammadi, N. Mousazadeh, et al., "Facile Preparation of Silver Based Radiosensitizers via Biomineralization Method for Enhanced In Vivo Breast Cancer Radiotherapy," *Scientific Reports* 13, no. 1 (2023): 15131.

65. Z. Ferdous and A. Nemmar, "Health Impact of Silver Nanoparticles: A Review of the Biodistribution and Toxicity Following Various Routes of Exposure," *International Journal of Molecular Sciences* 21, no. 7 (2020): 2375.

66. B. Dąbrowska-Bouta, G. Sulkowski, W. Strużyński, and L. Strużyńska, "Prolonged Exposure to Silver Nanoparticles Results in Oxidative Stress in Cerebral Myelin," *Neurotoxicity Research* 35 (2019): 495–504.

67. P. Aparajay and A. Dev, "Functionalized Niosomes as a Smart Delivery Device in Cancer and Fungal Infection," *European Journal of Pharmaceutical Sciences* 168 (2022): 106052.